Three-dimensional SOI-MEMS constructed by buckled bridges and vertical comb drive actuator

doi: 10.1109/JSTQE.2004.830616

Three-Dimensional SOI-MEMS Constructed by Buckled Bridges and Vertical Comb Drive Actuator

Minoru Sasaki, Danick Briand, Wilfried Noell, Nicolaas F. de Rooij, and Kazuhiro Hane

***Abstract*—A new method for realizing three-dimensional structures based on the standard silicon-on-insulator microelectromechanical systems is developed using vertically buckled bridges as structural elements. The vertical displacement, profile of the bridge, and obtainable accuracy of the displacement are examined. Using the lateral dimension control of the bridge and the supporting beams, the vertical positioning is realized based on the planer photolithography. As a demonstration, a vertical comb drive actuator is prepared and its performance is examined.**

***Index Terms*—Buckling, silicon-on-insulator microelectromechanical systems (SOI-MEMS), three-dimensional (3-D) structure, vertical comb drive actuator.**

I. Introduction

FABRICATION of microelectromechanical systems (MEMS) using a silicon-on-insulator (SOI) wafer is now a well-recognized technology. Compared to thin poly-Si films used in the surface micromachining, the bulk thick crystal Si (c-Si) device layer in the SOI wafer is advantageous for obtaining the rigid mirror with the optical grade flatness. At the cost of obtaining the robust mechanical elements, the driving using the microactuator becomes technical. Typical SOI-MEMS use the lateral movement [1]. The flexible spring in the lateral direction is obtained easily by designing beams with a narrow width (typically a few μm) in combination with the deep reactive ion etching (RIE) of Si [2]. The combination of such spring with the lateral comb drive actuator, which can be fabricated at the same time, keeps the fabrication process simple [3].

The in-plane layout is, however, limiting in the variations of the realizable optical setup and the actuator motion. Some applications require the vertical movement of the mirror. This is relatively difficult to realize in SOI-MEMS. In the field of the surface micromachining [4], the structural variation increases with the number of poly-Si structural layers. The fabrication process with the technologies available is depositing several poly-Si and SiO_2 layers necessary for realizing the structure. Many sophisticated mirror devices have complicated structures using many poly-Si layers [5]. According to the analogy, controlling the position of the device c-Si layer in SOI-MEMS is attractive to provide more variations in the structure. For optical scanners, vertical comb drive actuators are frequently used for rotating micromirrors. The paired combs have to be positioned at different heights. As for the bulk micromachining, the wafer bonding technique is an established approach for realizing the vertical comb drive actuator [6]–[9]. The delay mask technique is also useful [10]. As a straightforward method, Si dry etching is simply carried out from the front side and backside of the wafer [11]. The backside Si etching tends to become deep increasing the technical difficulty due to the limit of the delicate etching performance.

Another approach is to prepare the final structures using a post processing steps [12]. After the fabrication of rather planer structures keeping the process standard, some structures of the design are moved up vertically to a new position realizing the three-dimensional (3-D) structure. The well-known first approach is the surface micromachining using pin-jointed movable structures [13]. Many driving force has been tried for lifting up the structures, for example, microactuators [14], [15], stress accumulated in the metal film [16], [17], surface tension of photoresist [18], glass [19], solder [20], and so on [21]. Fundamentally, the used force is tensile. The compressive stress is avoided, since this will increase the risk of the adhesion to the underlying layer [22]. When the vertical comb drive actuator is considered, the post-processing approach is advantageous since the paired combs can be patterned from the single mask realizing the accurate relative position [23], [24]. However, when some parts are designed to be flexible for the large lifting distance, the overall device tends to become mechanically unstable. The locking mechanism after lifting is one strategy to stabilize the structure [16]–[18], [20]. This complicated mechanism will be possible for poly-Si surface micromachining. When the bulk Si material is used as the fabrication technology, the heat treatment has been examined for changing the structural shape [25], [26]. A stable structure realized by a simple fabrication process, which can be compatible with SOI-MEMS process, will be advantageous. Jeong *et al.* recently used the bending of the cantilever for generating the vertical combs [27].

In this paper, Si structures are lifted up realizing the 3-D structure of the SOI-MEMS by introducing the vertically buckled Si bridges. The vertical comb drive actuator is realized as a simple demonstration and its performance is examined.

II. Principle

Fig. 1 shows a schematic illustration that explains the principle. The bridge is made of Si and SiO_2 layers. When the underlying SiO_2 sacrificial layer is removed and the mechanical

Manuscript received October 19, 2003; revised April 4, 2004. This work was supported by the Venture Business Laboratory, Tohoku University.

M. Sasaki and K. Hane are with the Department of Nanomechanics Engineering, Tohoku University, Sendai 980-8579, Japan (e-mail: sasaki@hane.mech.tohoku.ac.jp).

D. Briand, W. Noell, and N. F. de Rooij are with the Institute of Microtechnology, University of Neuchatel, CH-2007 Neuchatel, Switzerland.

Digital Object Identifier 10.1109/JSTQE.2004.830616

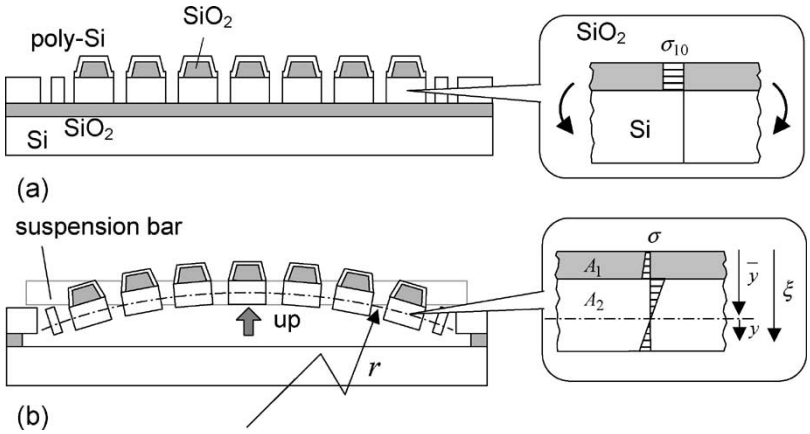

Fig. 1. Schematic illustration of the principle. The inset illustrates the stress distribution across the beam.

structure is released, the compressive stress accumulated inside the thermally grown SiO_2 film is no more supported. The bridge buckles vertically lifting its center as shown in Fig. 1(b). The suspension bars fix the bridge at its corners being allowed to rotate. Suspension bars are designed to have small spring constant for not disturbing the buckling motion of the bridge. This movement can be used for lifting a part of microstructures up to the new position. For the final release of the structure using the sacrificial layer etching, holes are opened inside the bridge. For minimizing the decrease of the buckling force, the area of the etching holes is minimized. The etching holes are distributed in a honeycomb in a structure with the aim of reducing the length of the underetching of the sacrificial layer. Supposing that the area of the Si and SiO_2 layers is the same, the bridge can be approximated by the simple composite beam. The thin poly-Si covering layer is ignored. According to the balance of force and moment after the buckling, the bridge will have an uniform radius of curvature. This radius of curvature r can be easily estimated. The following equation can be obtained from the balance of the force working at the cross-section of the bridge:

$$\int_{A_1} \sigma_1 dA + \int_{A_2} \sigma_2 dA = 0. \tag{1}$$

Here, A_1 and A_2 are the area covered by the SiO_2 and Si films [see inset of Fig. 1(b)], σ_1 and σ_2 are stresses inside the SiO_2 and Si films, respectively. Before buckling, σ_1 and σ_2 are σ_{10} and 0, respectively. σ_{10} is the initial compressive stress accumulated inside the SiO_2 film. In this study, the value used is 0.285 GPa, which is the moderate average of reported values obtained from the experiment [28]. Due to the buckling, this stress will be relaxed with the deflection

$$\sigma_1 = \sigma_{10} + \frac{E_1 y}{r}$$
$$\sigma_2 = \frac{E_2 y}{r} \tag{2}$$

where E_1 and E_2 are the Young's modulus of SiO_2 and c-Si. The coordinate y can be defined from the neutral axis inside the bridge

$$y = \xi - \overline{y} \tag{3}$$

where $\overline{y}$ is the position of the neutral axis, ξ is the coordinate along the y axis, and r has minus value in this condition. From the balance of the moment, another equation can be obtained

$$\int_{A_1} \sigma_1 y \, dA + \int_{A_2} \sigma_2 y \, dA = 0. \tag{4}$$

Unknown $\overline{y}$ and r can be numerically calculated from these two equations. Since the buckled bridge has the uniform radius of curvature r, the maximum displacement $y_{\max}$ at the center can be written as follows:

$$y_{\max} = \frac{l^2}{8r} \tag{5}$$

where l is the length of the bridge showing the square relation to $y_{\max}$.

III. Fabrication

An SOI wafer, with a Si device layer and a buried oxide layer 15 and 2-μm thick, is used. This wafer is thermally oxidized at 1100 °C obtaining a 1.97-μm-thick SiO_2 film [Fig. 2(a)]. The remained device Si thickness is estimated to be 14.1 μm. After the Cr deposition used as a hard mask against the HF wet etching, the SiO_2 layer is patterned as a mesh. Then, the wafer is covered by the 200-nm-thick poly-Si film grown at 600 °C [Fig. 2(b)]. The pinholes are suppressed by growing the film in two steps. This poly-Si and the underlying SiO_2 layers are partially removed for opening the contact electrodes [Fig. 2(c)]. At this step, the wafer has at least 2.4 μm height difference due to the SiO_2 and poly-Si layers. This is still not a serious problem for the spin coating and the standard patterning of the planer lithography. The subsequent processes are the same as those used in standard SOI-MEMS technology. The next patterning defines the device structure. For protecting the mesh-patterned SiO_2 film during the sacrificial SiO_2 layer etching, patterning a resist without misalignment is necessary for covering the entire SiO_2 region using poly-Si film. In our experiment, the alignment margin is 2.4 μm. After the continuous dry etching of poly-Si and c-Si [Fig. 2(d)], the sacrificial layer etching is carried out. When the bridge is released inside HF solution, the bridge automatically buckles to the vertical direction. This motion decreases the contact area and the adhesion possibility [Fig. 2(e)]

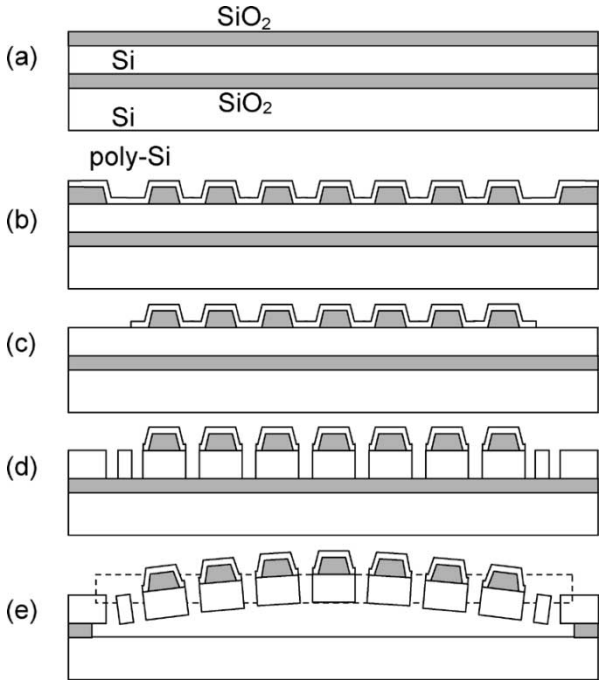

Fig. 2. Fabrication sequence of the buckled bridge and the vertical comb drive actuator.

[22]. The device is freeze-dried using the sublimation of cyclohexane. Being connected to the center part of bridges, the mirror is lifted up generating the vertical comb drive actuator and the space for the mirror rotation.

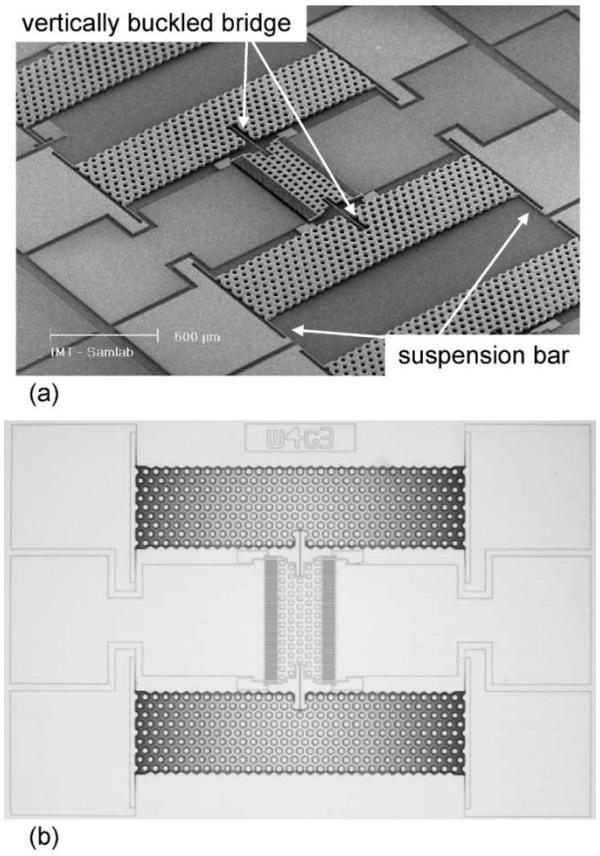

Fig. 3. Micrographs of one demonstrated structure observed by (a) scanning electron microscope and (b) optical microscope.

IV. Results

A. Buckled Bridge

Fig. 3(a) shows one fabricated structure. There are two parallel bridges, which buckles upward generating shallow arches. The bridge length is 1500 μm. The obtained vertical displacement is 26 μm. The displacement is measured using the confocal microscope. The center part is a rotational mirror with holes having the vertical comb drive actuator at both sides. The surrounding six rectangles are electrodes. The center mirror is connected to four electrodes via torsion bars and suspension bars. The two electrodes at the center are for driving. The bridge is aligned to the $\langle 100 \rangle$ direction of the (100) Si wafer, since this direction has smaller Young's modulus. Fig. 3(b) shows the optical micrograph of this device. By using the low magnification objective, the image brightness is sensitive to the tilt angle of the structure. The buckling profile of bridges and the twisting profile of suspension bars can be estimated from the image brightness. The suspension bars are not only twisted but also bended toward the bridge center due to the minute shrinkage of the total length of the bridge. Fig. 4 shows magnified views of combs lifted up by different displacements. Fig. 4(a)-(c) corresponds to the buckled bridge length of 900, 1200, and 1500 μm, respectively. The vertical displacement increases with the bridge length. The relative in-plane position between upper and lower combs is maintained. The measured lateral shift is < 0.15 μm in average showing the pure vertical shift and the balance of bridges. By preparing bumps at corners of the bridge as shown in Fig. 5, the possibility that adhesion occurs between the lifted part and the substrate can be reduced. The contact area reduces to the point in combination with the buckling motion of the bridge. No adhesion is observed during the process even though the maximum bridge is 2100 μm in length on the 2 μm thick sacrificial SiO_2 layer.

Fig. 6 shows the vertical (comb-to-comb) displacement as a function of the buckled bridge length. The solid line is the theoretical estimation using a simple composite beam model. The displacement reaches 52 μm when the buckled bridge length is 2100 μm. The vertical displacement can be controlled by the lateral design. The main factor is the bridge length. Experimentally, the minute difference of suspension bars (I- and T-shaped bars as shown in Fig. 5) is examined. This is for confirming the effect of the boundary condition. Both suspension bars have a width of 5 and a length of 145 μm and, therefore, have the same twisting spring constant. Since the T-shaped bar (bridge in T-shaped bar has a width of 5 and a length of 100 μm) allows the angular rotation at the base end of the straight bar, the boundary condition becomes more flexible especially for the lateral shift. For the vertical buckling of the bridge, corners of the bridge have to not only twist but also shift in the lateral direction as seen in Fig. 3(b). Open circles and dots correspond to bridges suspended by I- and T-shaped bars, respectively. The gray points show the difference between the experimental value and the theoretical estimation emphasizing the difference. T-shaped suspension bars give a slightly larger displacement. It is in between

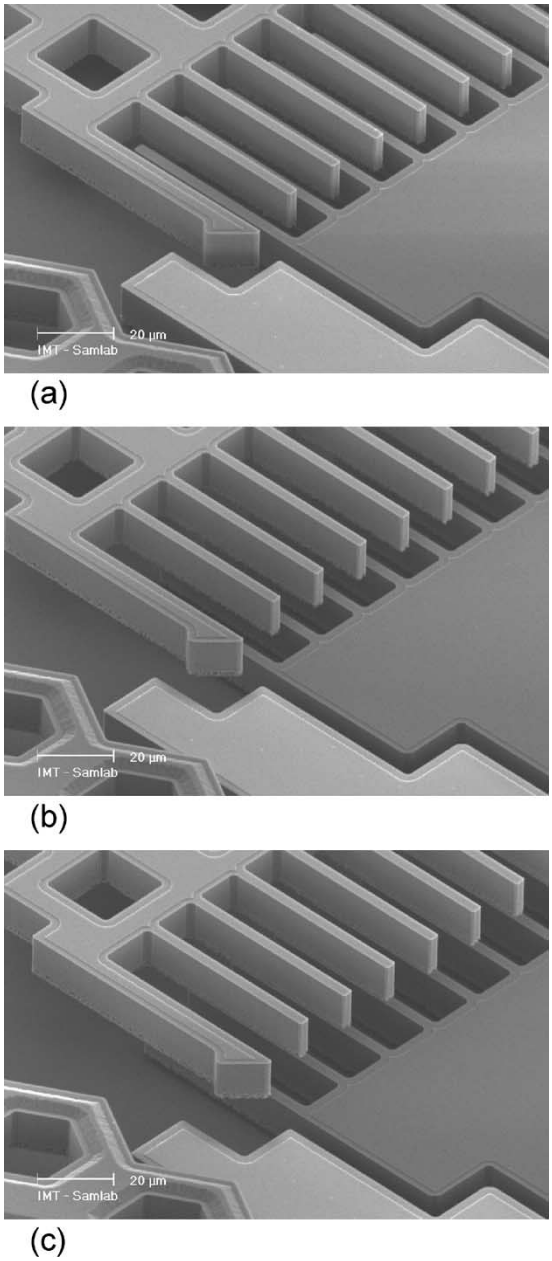

Fig. 4. Magnified image of realized vertical comb. The vertical lifting displacements are (a) 10 (b) 18, and (c) 26 μm.

1.5 to 6.8% in ratio compared to the total value of vertical displacement. The shorter bridge shows the larger increasing ratio when the I-shaped bar is replaced to T-shaped bar.

The longer bridge has a significant divergence in the displacement data. This can be attributed to the thickness variation of the device Si layer over the wafer. The specification of the Si device layer of the used SOI wafer is 15 ± 0.5 μm. Actually, the height difference between the underlying handle Si and the device Si is measured including the buried oxide thickness. This height difference is 17.3 μm at the center and 16.0 μm at the peripheral of $4''$ wafer. Since the thickness of 2 μm buried oxide layer is uniform on the order of a few %, this can be attributed to the local difference of the Si thickness. By setting the Si thickness to 15 ± 0.5 μm in the calculation, the change of the vertical displacement from the designed value is theoretically estimated. Fig. 7 presents the result. Including the value, the feature of Fig. 7 agrees well with the experimental data. The accuracy of the absolute displacement realized by the buckled bridge is mainly limited by the accuracy of the device Si thickness of the SOI wafer. When two bridges are prepared next to each other, their height difference will have a sub-μm level of accuracy, since they will have almost the same Si thickness.

Fig. 8 shows the cross-section of buckled bridges having a simple straight structure as shown in the inset. The values of the vertical displacement are smaller than those of bridges shown in Figs. 3 and 6. This can be attributed to the decrease of the area ratio of SiO_2 layer to Si layer. Bridge profiles are almost the same, overlapping each other, showing almost the same radius of curvature. Note that the 2100-μm-long bridge shows a relatively larger radius of curvature. This can be attributed to the stiffness of the suspension bars compared to the long buckled bridge having a low spring constant.

B. Realized Vertical Comb Drive Actuator

Fig. 9 shows the mirror rotation angle as a function of the driving voltage. The mirror and the underlying handling Si are grounded. The positive voltage is applied to a driving electrode. The initial comb-to-comb distance is the parameter. The mirror size is 202×578 μm^2. The comb finger is 55 μm in length and 3.4 μm in width. The number of comb pairs is 38.5 for one side. The gap between combs is 3.6 μm. The torsion bar is 2.4 μm in width and 200 μm in length. Since the device Si layer is 14.1 μm in thickness, combs overlap each other from the beginning when the initial comb-to-tomb distances are 4.2 and 10 μm. The larger 10 μm comb-to-comb distance generates the larger rotation angle. With the larger vertical shift, the vertical force is efficiently generated even though the same driving voltage is applied. The mirror rotation follows a nearly linear relation as a function of the driving voltage. When the comb-to-comb distance increases to 18 μm (a vertically 3.9 μm gap is generated between combs), the curve becomes S-shape. A mirror rotation up to 4.5° is obtained at the driving voltage of 55 V. In this layout, the combs begin to overlap each other when the mirror rotation reaches about 1.5°. After this, the curve changes to a nearly linear relation having a larger slope as a function of the driving voltage. And then, the mirror rotation saturates at around 4.5° over 55 V. The pull-in motion is suppressed. As for the low driving voltage, the electrical field will be weak due to the large gap between the combs until the combs overlap each other. The setup with a 10-μm comb-to-comb distance is advantageous at the low driving voltage, since the increasing ratio of the mirror angle is larger. When the vertical comb-to-comb distance further increases to 26 μm, the mirror rotation is not efficiently obtained due to the weak electrical field. Although the electrical field increases by applying a higher driving voltage, the instability of the pull-in motion limits the controllable mirror rotation.

Due to the lateral force unbalance at the large driving voltage, the mirror rotates in-plane direction generating a short circuit from comb to comb. Since this phenomenon occurs from about 80 V for the device with a 26-μm comb-to-comb distance, the stable mirror rotation is limited to 2°. The inset of Fig. 10 illustrates the typical motion. Fig. 10 plots the voltage at which

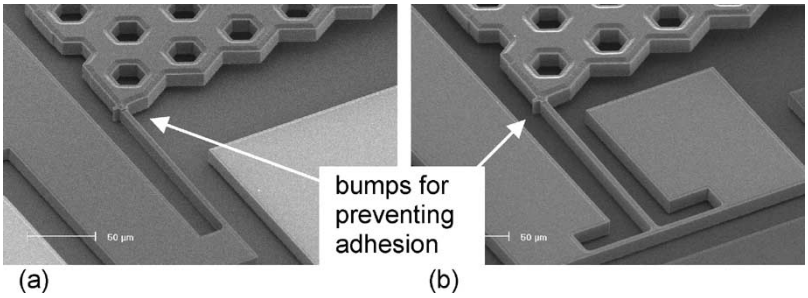

Fig. 5. (a) I- and (b) T-shaped suspension bars. The bump is $4 \times 4\ \mu\mathrm{m}^2$ in design.

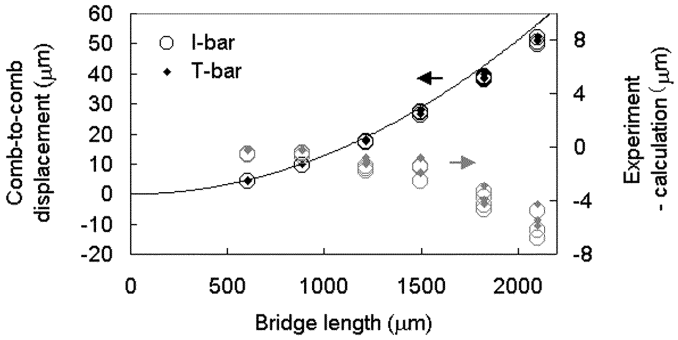

Fig. 6. Vertical displacement as a function of the buckled bridge length. Gray colored data are the difference between the experimental and theoretical values.

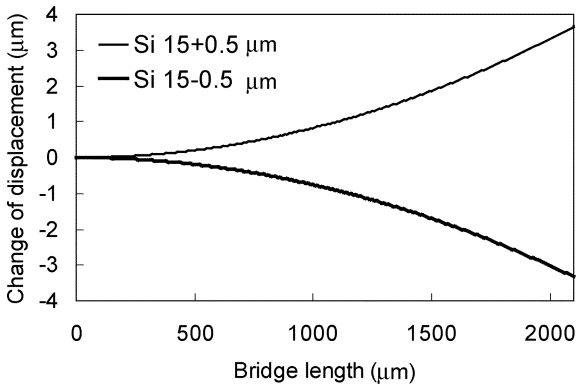

Fig. 7. Change of the vertical displacement from the designed value considering the thickness change caused by the quality limit of the SOI wafer. The designed thickness of the SOI device layer and the thermally oxidized layer are 15 and 2 μm, respectively.

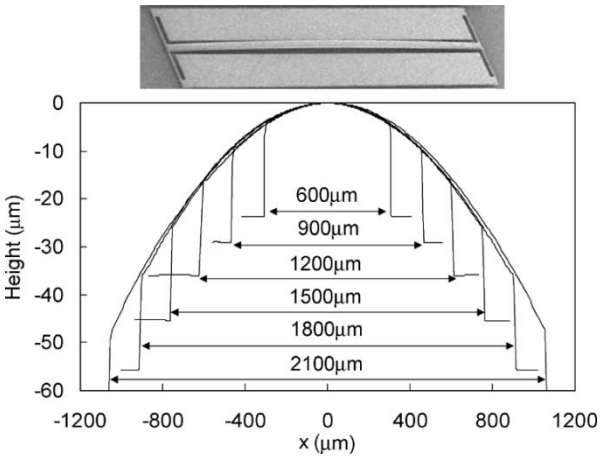

Fig. 8. Cross-sectional profiles of buckled bridges having the structure as shown in the inset.

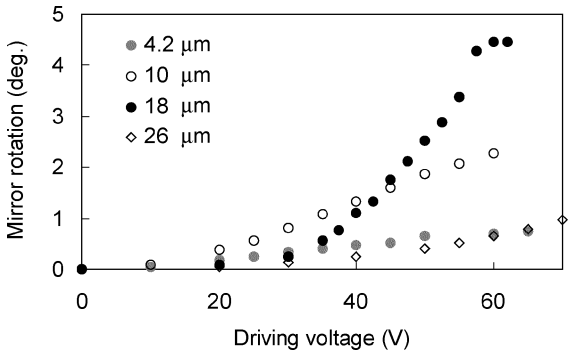

Fig. 9. Mirror rotation angle as a function of driving voltage with the different initial comb-to-comb vertical distance.

the in-plane rotation was observed. Although there is a significant dispersion in data, this unstable voltage (or the stable operation region) increases with the initial comb-to-comb distance. When the overlapping comb area increases with the mirror rotation leading to large cross-axis forces, the sudden snapping in-plane rotation of the mirror is generated. When the vertical shift is 4.2 μm, the in-plane rotation is observed even at about 40 V. Notice that the data for a 0-μm comb-to-comb distance (without buckling) is different in the mirror movement due to the limited open space. The mechanical stopper protecting the electrical shortage is included in the mirror as seen in the inset of Fig. 10. For actuators having the large initial comb-to-comb distance ($\geq 18\ \mu$m), this protection does not work efficiently resulting in the break down of the torsion bar. Combs having the lateral gaps of 4.6 μm are also examined. The stable region increases with the lateral gap, at the cost of decrease of the driving force for the mirror.

Fig. 11 shows the parasitic downward movement of the buckled bridge when the driving force is applied for the mirror rotation. This parasitic movement is obtained measuring the displacement at the center of the buckled bridge. The ratio between the parasitic displacement and the mirror rotation is measured as a function of the spring constant of the buckled bridge. The spring constant was experimentally measured using the stylus profiler (KLA-Tencor, P-15) by measuring the buckled bridge height changing the contact force. The longer bridge corresponds to the smaller spring constant. According to the data, the parasitic displacement is related to the balance

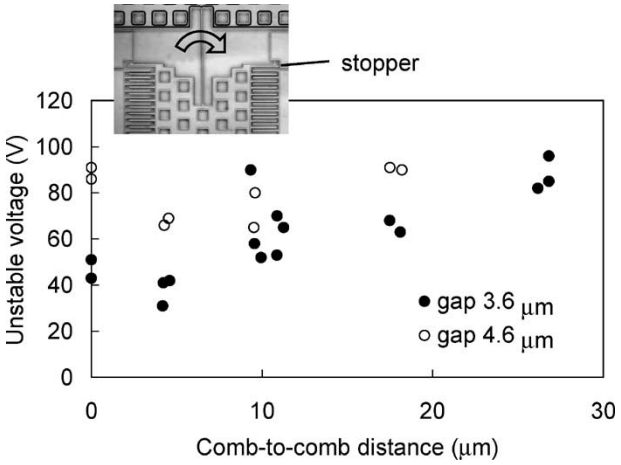

Fig. 10. Driving voltage at which the in-plane rotation of the mirror occurs. Devices with 26 μm comb-to-comb distance and 4.6 μm gap have an unstable voltage larger than 100 V.

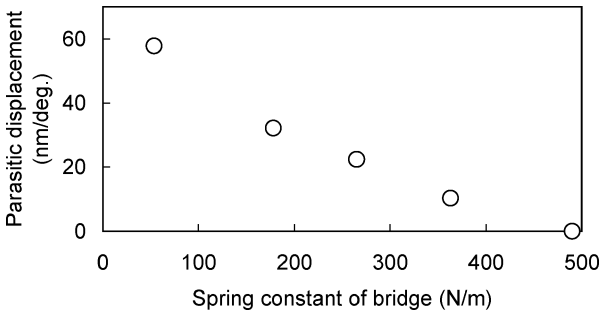

Fig. 11. Measured parasitic displacement at the center of the buckled bridge during the mirror rotation. The bridges are suspended by the I-shaped bar.

of spring constants between the bridge and the twisting bar. The buckled bridge having longer length needs the wider width for obtaining a larger spring constant. The actuator generating mirror rotation of 4.5° are supported by the bridge with the spring constant of 178 N/m. The ratio is 32 nm/°. As for the demonstrated device, the parasitic displacement is suppressed at sub-μm level.

Fig. 12 shows the typical frequency response. Fig. 12(a) is obtained measuring the displacement at the mirror including the displacement from the 900-μm-long bridge. Measuring the response with the phase relation at both sides of the mirror, peaks at around 7 kHz are confirmed to correspond to the mode of mirror rotation. Black and gray curves are obtained from devices with bridges suspended by I- and T-shaped bars, respectively. The smaller peaks at about 27 kHz correspond to the mode of the vertical bending of the bridge. Fig. 12(b) shows this resonant frequency as a function of bridge length. The resonant frequency of the buckled bridges with T-shaped bars is smaller by 0.5–1.6 kHz compared to those with I-shaped bars. The resonant frequency of bridges at 9.4–31 kHz is larger than that of the mirror rotation at around 7 kHz.

V. Conclusion

A method for realizing 3-D structures in SOI-MEMS is developed introducing the vertically buckled bridges. The compressive stress of the thermally grown SiO_2 film is used

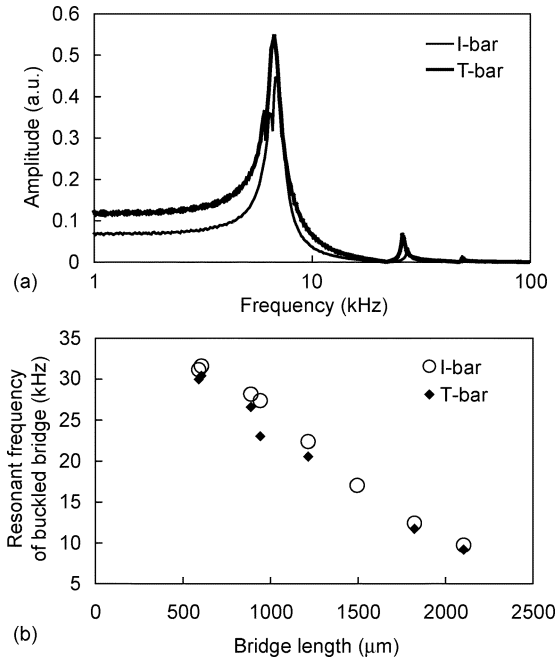

Fig. 12. (a) Typical frequency response of the mirror lifted by the buckled bridges. (b) Plot of the resonant frequency as a function of the bridge length. Lack of some data is attributed to the damage during the operation, which changes the characteristics.

for the buckling. The vertical displacement up to 50 μm is confirmed using 14.1-μm-thick Si device layer. The simple estimation of the buckling displacement agrees well with the experimental data. This technique is compatible with the standard planer lithography. A vertical comb drive actuator is demonstrated, and its performance is measured confirming the rigidity of the buckled bridge. The driving performance of the vertical comb drive actuator changes depending on the initial comb-to-comb distance. For obtaining larger rotation of the mirror, the initial comb-to-comb distance a little larger than the device Si thickness is appropriate. The demonstrated mirror rotation is 4.5° at the driving voltage of 55 V showing S-shaped curve against the driving voltage. For the driving at low voltage, the vertical distance smaller than the device Si thickness is appropriate showing a nearly linear relation.

Acknowledgment

The authors would like to thank related group members with the Institute of Microtechnology, University of Neuchatel, especially T. Akiyama, W. Sun, T. Overstolz, M. Zickar, G. Mondin, and C. Marxer, for exciting discussions.

References

[1] C. Marxer and N. F. de Rooij, "Micro-optomechanical 2 × 2 switch for single-mode fibers based on a plasma-etched silicon mirror and electrostatic actuation," *J. Lightwave Technol.*, vol. 17, pp. 2–6, 1999.

[2] W. Noell, P.-A. Clerc, L. Dllmann, B. Guldimann, H.-P. Herzig, O. Manzardo, C. R. Marxer, K. J. Weible, R. Dandliker, and N. de Rooij, "Applications of SOI-based optical MEMS," *IEEE J. Select. Top. Quantum Electron.*, vol. 8, pp. 148–154, Jan./Feb. 2002.

[3] R. Legtenberg, A. W. Groeneveld, and M. Elwenspoek, "Comb-drive actuators for large displacements," *J. Micromech. Microeng.*, vol. 6, pp. 320–329, 1996.

[4] R. T. Howe, "Surface micromachining for microsensors and microactuators," *J. Vac. Sci. Technol., B*, vol. B6, pp. 1809–1813, 1998.

[5] R. S. Muller and K. Y. Lau, "Surface-micromachined microoptical elements and systems," *Proc. IEEE*, vol. 86, pp. 1705–1720, Aug. 1998.
[6] J. T. Nee, R. A. Conant, R. S. Muller, and K. Y. Lau, "Lightweight, optically flat micromirrors for fast beam steering," in *Proc. IEEE/LEOS Int. Conf. Optical MEMS*, 2000, pp. 9–10.
[7] H. Wada, D. Lee, U. Krishnamoorthy, S. Zappe, and O. Solgaard, "Process for high speed Micro Electro Mechanical Systems (MEMS) scanning mirrors with vertical comb drives," *Jpn. J. Appl. Phys.*, vol. 41, pp. L899–L901, 2002.
[8] J.-H. Lee, Y.-C. Ko, B.-S. Choi, J.-M. Kim, and D. Y. Jeon, "Bonding of silicon scanning mirror having vertical comb fingers," *J. Micromech. Microeng.*, vol. 12, pp. 644–649, 2002.
[9] J.-H. Lee, Y.-C. Ko, D.-H. Kong, J.-M. Kim, K. B. Lee, and D.-Y. Jeon, "Design and fabrication of scanning mirror for laser display," *Sens. Actuators, A*, vol. A96, pp. 223–230, 2002.
[10] V. Milanovic, G. A. Matus, T. Cheng, and B. Cagdaser, "Monolithic high aspect ratio two-axis optical scanners in SOI," in *Proc. 16th IEEE Int. Conf. Micro Electro Mechanical Systems*, 2003, pp. 255–258.
[11] O. Tsuboi, Y. Mizuno, N. Kouma, H. Soneda, H. Okuda, S. Ueda, I. Sawaki, and F. Yamagishi, "A rotational comb-driven micromirror with a large deflection angle and low drive voltage," in *Proc. 15th IEEE Int. Conf. Micro Electro Mechanical Systems*, 2002, pp. 532–535.
[12] W. Fang and J. A. Wickert, "Post buckling of micromachined beams," *J. Micromech. Microeng.*, vol. 4, pp. 116–122, 1994.
[13] L. Y. Lin, S. S. Lee, K. S. J. Pister, and M. C. Wu, "Micro-machined three-dimensional micro-optics for integrated free-space optical system," *IEEE Photonics Technol. Lett.*, vol. 6, pp. 1445–1447, 1994.
[14] J. R. Reid, V. M. Bright, and J. T. Butler, "Automated assembly of flip-up micromirrors," *Sens. Actuators, A*, vol. A66, pp. 292–298, 1998.
[15] H. Toshiyoshi, W. Piyawattanametha, C.-T. Chan, and M. C. Wu, "Linearization of electrostatically actuated surface micromachined 2-D optical scanner," *J. Microelectromech. Syst.*, vol. 10, pp. 205–214, 2001.
[16] R. Giles and D. Bishop, "Lightwave micromachines in optical networks," in *Proc. IEEE/LEOS Int. Conf. Optical MEMS*, 2000, Post deadline paper.
[17] Y.-P. Ho, M. C. Wu, H.-Y. Lin, and W. Fang, "A robust and reliable stress-induced self-assembly mechanism for optical devices," in *Proc. IEEE/LEOS Int. Conf. Optical MEMS*, 2002, pp. 131–132.
[18] R. R. A. Syms, C. Gormley, and S. Blackstone, "Improving yield, accuracy and complexity in surface tension self-assembled MOEMS," *Sens. Actuators, A*, vol. A88, pp. 273–283, 2001.
[19] R. R. Syms, "Rotational self-assembly of complex microstructures by the surface tension of glass," *Sens. Actuators, A*, vol. A65, pp. 238–243, 1998.
[20] K. F. Harsh, V. M. Bright, and Y. C. Lee, "Solder self-assembly for three-dimensional microelectromechanical systems," *Sens. Actuators, A*, vol. A77, pp. 237–244.
[21] M. Ishimori, J. H. Song, M. Sasaki, and K. Hane, "Si-wafer bending technique for a three-dimensional microoptical bench," *Jpn. J. Appl. Phys.*, pt. 1, vol. 6B, pp. 4063–4066, 2003.
[22] R. Maboudian and R. T. Howe, "Adhesion in surface micromechanical structures," *J. Vac. Sci. Technol.*, vol. B15, pp. 1–20, 1997.
[23] P. R. Patterson, D. Hah, H. Nguyen, H. Toshiyoshi, R. Chao, and M. C. Wu, "A scanning micromirror with angular comb drive actuation," in *Proc. 15th IEEE Int. Conf. Micro Electro Mechanical Systems*, 2002, pp. 544–547.
[24] W. Piyawattanametha, P. R. Patterson, D. Hah, H. Toshiyoshi, and M. C. Wu, "A 2-D scanner by surface and bulk micromachined angular vertical comb actuators," in *Proc. IEEE/LEOS Int. Conf. Optical MEMS*, 2003, pp. 93–94.
[25] E.-H. Yang and H. Fujita, "Reshaping of single-crystal silicon microstructures," *Jpn. J. Appl. Phys.*, vol. 38, pp. 1580–1583, 1999.
[26] J. Fruhauf, E. Gartner, and E. Jansch, "Silicon as a plastic material," *J. Micromech. Microeng.*, vol. 9, pp. 305–312, 1999.
[27] K.-H. Jeong and L. P. Lee, "A novel fabrication method of a vertical comb drive using a single SOI wafer for optical MEMS applications," in *Proc. 2003 Int. Conf. Solid-State Sensors and Actuators*, 2003, 3E74P, pp. 1462–1465.
[28] W. Fang and J. A. Wickert, "Post buckling of micromachined beams," *J. Micromech. Microeng.*, vol. 4, pp. 116–122, 1994.

Minoru Sasaki received the B.E. and Dr.Eng. degrees from Nagoya University, Nagoya, Japan, in 1993 and 1995, respectively.

In 1996, he became a Research Fellow with the Japan Society for the Promotion of Science. Since 1996, he has been a member of the Department of Mechatronics and Precision Engineering, Tohoku University, Sendai, Japan, where he is currently Associate Professor. His research interests include the research and development of optical MEMS including sensors.

Danick Briand received the B.Eng. and M.A.Sc. degrees in engineering physics from Ecole Polytechnique, Montreal, QC, Canada, in collaboration with the Laboratoire des Materiaux et du Genie Physique, Grenoble, France, in 1995 and 1997, respectively, and the Ph.D. degree in the field of micro-chemical systems from the Institute of Microtechnology, University of Neuchatel, Neuchatel, Switzerland, in 2001,

He is currently a Team Leader at the Institute of Microtechnology, University of Neuchatel, where he is in charge of European and industrial projects, of the supervision of doctoral students and has teaching assignments. His research interests in the field of microsystems include wafer bonding, micro-combustion, and the integration, packaging, and reliability of micro-chemical sensors.

Wilfried Noell received the Dipl. degree in physics from the Technical University of Darmstadt (TUD), Darmstadt, Germany, in 1994. His diploma thesis was a joint work between the Applied Optics Group of the Physics Department, TUD, and the Research and Technology Center (FTZ), Deutsche Telekom on integrated optical waveguides based on InP. He received the Ph.D. degree in physics from the University of Ulm, Germany, in 1998. His graduate work on the development of a microfabricated optical near-field sensor was pursued externally at the Institute for Microtechnology Mainz, Germany.

Since 1998, he has been with the Institute of Microtechnology, University of Neuchatel, Switzerland. After working for more than two years on tools for nanoscience, he became responsible for the group's activities on optical microsystems in the beginning of 2001.

Nicolaas F. de Rooij joined the Institute of Microtechnology, University of Neuchatel, Switzerland (IMT UNI-NE), as a Professor and Head of the Sensors, Actuators, and Microsystems Laboratory, in 1982. From October 1990 to October 1996, he was acting as Director of the IMT UNI-NE. He lectured as the Swiss Federal Institute of Technology, Zurich, and since 1989, he has been a Part-time Professor at the Swiss Federal Institute of Technology, Lausanne. He was a member of the steering committee of the International Conference on Solid-State Sensors and Actuators and of Eurosensors, and acted as European Program Chairman of Transducers, in 1987, and General Chairman of Transducers, in 1989. His research activities include microfabricated sensors, actuators, and microsystems.

Mr. de Rooij is a member of the editorial boards for the IEEE JOURNAL OF MICROELECTROMECHANICAL SYSTEMS, *Sensors and Actuators*, and *Sensors and Materials*.

K. Hane received the M.S. and Dr.Eng. degrees from Nagoya University, Nagoya, Japan, in 1980 and 1983, respectively.

From 1983 to 1994, he was a Member of the Department Electronic-Mechanical Engineering, Nagoya University. From 1985 to 1986, he was a Guest Researcher with the National Research Council of Canada. Since 1994, he has been a Professor with the Department of Mechatronics and Precision Engineering, Tohoku University, Sendai, Japan, and is currently engaged in the research and development of microsensors and optomechanical systems.